Efficient Single-Cell Mechanical Measurement by Integrating a Cell Arraying Microfluidic Device With Magnetic Tweezer

Xiaoqing Tang, Xiaoming Liu, *Member, IEEE*, Pengyun Li, Dan Liu, Masaru Kojima, Qiang Huang, *Fellow, IEEE*, and Tatsuo Arai, *Fellow, IEEE*

***Abstract*—Cell stiffness is an essential label-free biomarker used to diagnose and sort cells at the single-cell level. Here, we integrated magnetic tweezers on an efficient cell arraying microfluidic device to evaluate the mechanical properties of single cells. Two motion modes under pulsed electromagnetic fields have been proposed for magnetic beads. They were magnetically actuated to approach the measuring cells at a distance in rotation mode and move experimentally with the maximal velocity of 23 μm s^{-1} under a rotating magnetic field of 45 Hz and 45 mT. In contrast, the magnetic beads were driven at close range in translation mode to approach and apply extrusion pressure on the target cells under a locally constant magnetic field gradient. The simulation results of the fluid field caused by the moving bead revealed the difference distribution in velocity and pressure under two motion modes, proving the rationality of the motion mode setting. Experimentally, Hela cells and C2C12 cells arrayed in the microfluidic device were physically squeezed by magnetic tweezers, and cell stiffness was measured. Compared to the measurement results with AFM, the proposed method used to measure Young's modulus of the cells was thought to be dependable. We envision the proposed on-chip platform integrated with the magnetic tweezer could show a potential application for the efficient and flexible measurement of biomechanical properties in the future.**

***Index Terms*—Magnetic tweezer, magnetic control, microfluidic device, mechanical measurement, cell stiffness.**

I. Introduction

CANCER, as the leading cause of death worldwide, has become the world's biggest killer within just a few decades. Consequently, more and more researches have been conducted to evaluate cancer disease. With the development of life sciences, different variations in the physical properties of cells, including size, shape, stiffness, and optical properties, have been used as biomarkers for cancer cell biophysics [1]–[4]. As one example of these characteristics, cell stiffness has attracted attention. It is proved related to the invasiveness of cancer cells, which is one of the most important features of cancer cells [5]–[8]. For example, it is reported that Young's modulus of the highly invasive human breast cancer cell MDA MB 231 is lower than that of the noninvasive cancer cell line MCF 7, which is further lower than that of the benign cell MCF 10 A [5]. In addition, certain studies have indicated that Young's modulus of HeLa cells is much higher than most of the other cancer cell lines [6].

A wide range of techniques has been developed to enable the characterizing of the cell mechanics experimentally. Atomic force microscopy (AFM) emerged as a versatile method to evaluate stiffness based on the deformation and reaction force of cells under external force extrusion [9]–[12]. As a more recent development, Liu *et al.* provide a comprehensive review of recent advances in the use of AFM to characterize the biomechanical properties of multi-scale biological samples, ranging from the molecule, cell to tissue levels [13]. Mandar *et al.* studied the stiffness measurements using AFM on cellular mechanoadaptation to substrate mechanical properties [14]. Additionally, optical tweezers are another powerful tool to much employed in the measurement of mechanical characteristics of micron-scale objects, which take effect by applying force and deformation on the magnitude of picoNewtons (pN) and nanometers (nm), respectively [15]- [18]. For instance, Tan *et al.* assessed the mechanical properties of human red blood cells under different osmotic conditions with optical tweezers [16]. Edward J *et al.* measured the mechanical characterization of Jurkat Cells before and after ART treatment using optical tweezers [18]. Both of the above could serve as an efficient and highly quantitative method for measuring mechanical properties. However, a low-throughput property of them limits large-sample studies for a single cell, which is essential in practical applications.

In addition, some methods that evaluate cell properties based on cell behavior without giving a direct excitation were also well developed. Tsai group proposed a series of researches on cell stiffness measurement using μ-channel by analyzing the two-phase motion of cells with a high-speed vision system

Manuscript received October 15, 2020; accepted February 22, 2021. Date of publication March 1, 2021; date of current version March 18, 2021. This letter was recommended for publication by Associate Editor D. Cappelleri and Editor X. Liu upon evaluation of the reviewers' comments. This work was supported in part by the National Natural Science Foundation of China under Grants 61903039 and 61873037, in part by the China Postdoctoral Science Foundation (BX20190035, 2020M680015) and in part by the Grant-in-Aid for Scientific Research (19H02093) from the Ministry of Education, Culture, Sports, Science and Technology of Japan. *(Corresponding author: Xiaoming Liu.)*

Xiaoqing Tang, Xiaoming Liu, Pengyun Li, Dan Liu, Qiang Huang, and Tatsuo Arai are with the Key Laboratory of Biomimetic Robots and Systems, Ministry of Education, State Key Laboratory of Intelligent Control and Decision of Complex System, Beijing Advanced Innovation Center for Intelligent Robots and Systems, and School of Mechatronical Engineering, Beijing Institute of Technology, Beijing 100081, China (e-mail: txq4996@163.com; liuxiaoming555@bit.edu.cn; lpyifendou@163.com; 3120185104@bit.edu.cn; qhuang@bit.edu.cn; tarai118@jcom.zaq.ne.jp).

Masaru Kojima is with the Department of Materials Engineering Science, Osaka University, Osaka 560-8531, Japan (e-mail: kojima@cheng.es.osaka-u.ac.jp).

Digital Object Identifier 10.1109/LRA.2021.3062793

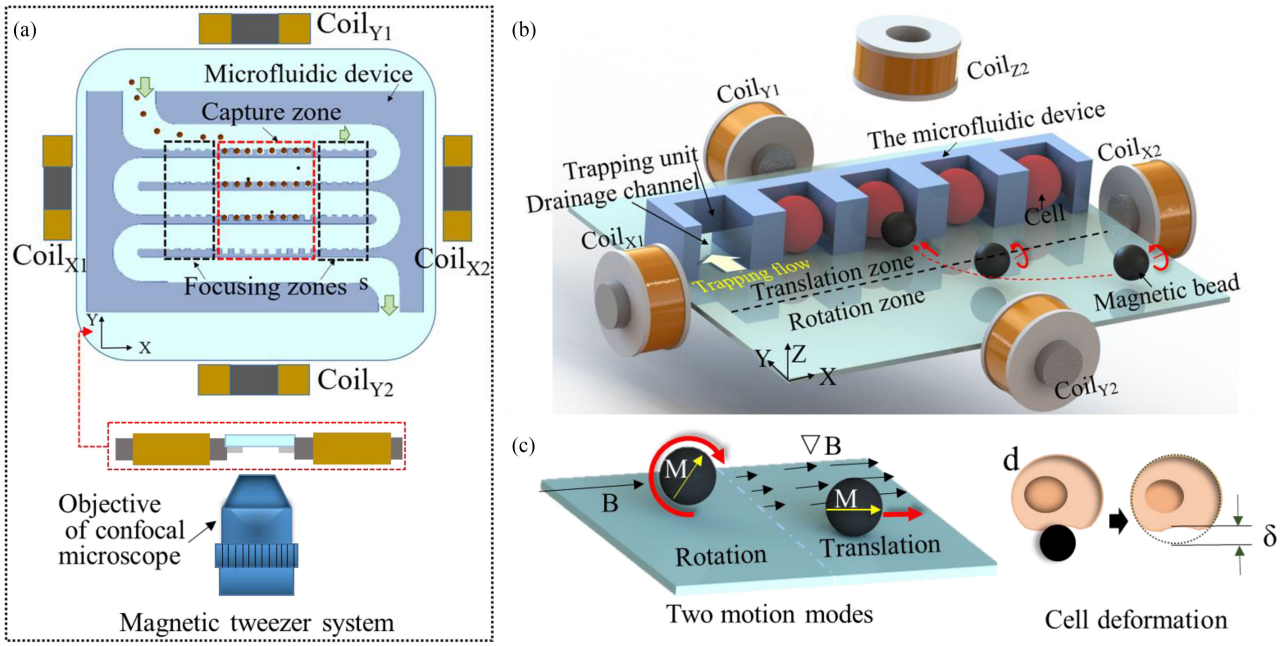

Fig. 1. (a) 2D magnetic tweezer system based on the efficient microfluidic device under the confocal microscope. (b) 3D magnetic tweezer system, including four magnetic coils in X-Y plane and a vertical coil along Z direction. The process of the magnetic bead to approach the cell with two motion modes is showed in the central platform. (c) Moving schematic of rotation mode in constant magnetic flux density and translation mode in magnetic gradient. (d) Cell deformation under extrusion force induced by the magnetic bead.

[19]–[22]. Adamo *et al.* employed the electrical impedance of cells to acquire the transit time of cells through a narrow channel then assess the cell deformability [23]. Hydrodynamic stretching and cell deformation have been demonstrated for mechanical phenotyping of cells by Gossett *et al.* [24]. A novel chip for automated cell deformation monitoring of erythrocyte with filter design was developed by Youn *et al.* [25]. The microfluidic chip was applied to measure the mechanics of breast cancer cells to make sure if the cells are malignant or not [26]. Those approaches above have led to a dramatic increase in high throughput analysis. However, the statistic of stiffness acquired from entry and transit time of cell in μ-channel can get affected by the size of cells and frictional properties of the contraction wall, resulting in a semi-quantitative analysis [27].

Therefore, there has been a general lack of approaches to measuring cellular stiffness properties with high throughput and high precision. Notably, two impressive apparatuses of a magnetic tweezer system and microfluidic device have been observed. Magnetic micromanipulation has recently promoted the development of biophysics applications featuring untethered control, high precision, and noninvasiveness [28]–[30]. Furthermore, as the high-throughput and high-efficiency device to immobilize and array single cells, the microfluidic chip is widely accepted in the single-cell analysis [31], [32]. Considering these researches, in this letter, we integrated a magnetic tweezer system with a high-throughput Lab on Chip (LOC) devices designed in a previously published work [33] to measure cellular stiffness, as schematically illustrated in Fig. 1. Two moving modes of rotation and translation were analyzed in the process of the magnetic bead moving to the cell surface. Accordingly, force modeling and calibration were carried out to understand the control mechanism. Finally, the cells were physically squeezed by magnetic beads, and cell stiffness was measured quantitatively.

II. Design and Fabrication

A. Single-Cell Arraying

A microfluidic device was designed to trap single cells. The device contains several rows with turning zones connecting them, and every row consists of the capture zone and the focusing zone on both ends of each row. In the capture zone, each trapping unit for a single cell has a drainage channel (Fig. 1(b)), so a pushing force is generated on the cells as the fluid flows through it. Once a trapping unit is occupied, and the cell occludes the entrance of the trapping unit, the trapping flow will continue through the adjacent parallel sub-pathway. As a result, cells are isolated and immobilized sequentially into a dense array of separate trapping units. Many focusing units whose chambers are smaller than the trapping units (Fig. 1(a)) are in the focusing zones. As cells passing by the focusing zones along the wide main channel, the focusing units can guide them to focus toward the entrance of the sub-pathways in the downstream row, but not used to capture single cells. Therefore, when the suspension flows into the device and through the main pathway, cells can be easily introduced into the unoccupied trapping units. Besides, the microfluidic device structure can be easily scalable for multiple cells and other types of cells with different dimensions by stretching the capture unit length. Correspondingly, other design variables of the microchannel structure should be adjusted to keep a proper fluid-resistant ratio for a high trapping efficiency. After optimizing structure parameters and the inlet flow velocity

of the microchannel, the capture efficiency of single cells by the proposed device was up to 97%, and the shear force on the cell in the trapping unit can be remained low to keep structural integrity of the cells and cell viability.

The microfluidic device was fabricated in PDMS by soft lithography method. A master mold was produced by patterning SU-8 photoresist (Switzerland Gersteltec 1050 and 1070) on a silicon wafer using standard two-layer photolithography. Liquid PDMS mixed with a curing agent (ratio of 10:1) was cast on the mold and cured for 2 h in a convection oven at 65°C for complete cross-linking. The PDMS microchannel was then irreversibly sealed with the glass after exposure to oxygen plasma for 60 s using vacuum plasma processing instrument.

B. Compact 3D Magnetic Tweezer

Fig. 1(a) and Fig. 1(b) sketches the configuration of a compact magnetic tweezer system, including five magnetic coils and the center operating platform of a microfluidic device. Among five magnetic coils, there are two pairs of coils distributing in the horizontal plane, which are equipped with the soft-magnetic and high-permeability material inside. Besides, another coil is equipped on the top of the center operating platform without the soft-magnetic material inside, which allows some space for light in the Z direction to pass through. Thus, the number of its turns is designed to be larger than that of others in order to make up for the lack of magnetic flux density. Additionally, to obtain the maximum magnetic flux density and magnetic field gradient, the four soft-magnetic materials distributing in the horizontal plane should be placed as close as possible to the platform. The motion of magnetic beads and the measurement of mechanical properties of cells are all carried out in the center operating platform, based on the PDMS microfluidic device of cell immobilization.

On the one hand, the magnetic tweezer system is typically designed to have a homogenous, gradient-free magnetic field in the center of magnetic coils when an alternating current is applied. On the other hand, the system is used to produce a magnetic field with a certain gradient when a constant current is applied to a coil in the X-Y plane.

C. Mechanical Measurement of Single Cell

The experimental process of the mechanical measurement of a single cell consists of two phases: the preparation works in microfluidic devices and the movement controlling of magnetic beads (Fig. 2). Firstly, to exhaust air in the whole channels and prevent the adhesion of the microstructure, the PBS solution is pumped into the microfluidic channel, and then cell suspension is loaded. After single cells are immobilized in all trapping units, a very low-density magnetic bead suspension dissolved in deionized water is vibrated in the ultrasonic cleaner for a uniformly distributed solution. They should then be injected into the microfluidic device and stopped when the beads load on the main channel. Once the magnetic beads are stable in their original position after a few seconds, they will be driven to move to the surface of the target cells and then give the extrusion force to the cell under the magnetic field. The motion modes and position of beads are controlled by regulating the driving currents in the coils, based on visual feedback from the confocal laser scanning microscope (CLSM). Once the bead contacts with the target cell, the deformation under extrusion pressure will be recorded by high-resolution confocal imaging, then the stiffness measurement could be conducted and analyzed quantitatively (Fig. 1(d)). Meanwhile, the magnetic force exerted on the bead is also controlled by adjusting the current in the coils. Subsequently, the magnetic bead was controlled to leave the cell surface and continue to test until the complete recovery of the cell deformation.

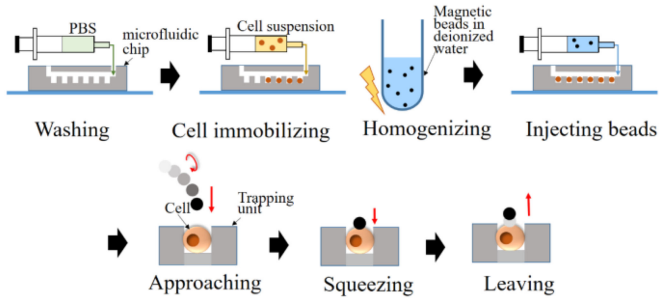

Fig. 2. The experimental process of mechanical measurement of single cell.

III. Motion Controlling

A. Motion Modes: Rotation and Translation

As schematically illustrated in Fig. 1(b) and Fig. 1(c), there are two kinds of motion modes used to control magnetic beads. One of them is the most noted actuation method that applies a magnetic field gradient $\bigtriangledown B$ to generate a driving force on the magnetic beads. The force is proportional to the local field gradient and pointed toward the regions of a higher magnetic field, which can be described as

$$\vec{F} = \vec{M} \cdot \left(\vec{\nabla} B\right) \tag{1}$$

where M is the net magnetic moment of the magnetic beads, B is the magnetic flux density. Another actuation method is to exert torque on magnetic beads by a rotating magnetic field with constant and uniform magnetic strength in space. The torque tends to rotate and align the bead moment with the direction of the external field, which is donated as

$$\vec{\tau} = \vec{M} \times B \tag{2}$$

The rotational actuation on magnetic beads can precisely control the torque, orientation, and angular velocity of magnetic beads with the applied function signal. The governing equations of the magnetic fields generated by the 3D coil system can be described as

$$B(t) = \begin{bmatrix} B_x(t) \\ B_y(t) \\ B_z(t) \end{bmatrix} = \begin{bmatrix} A\cos(\alpha(t))\cos(\theta(t)) \\ A\cos(\alpha(t))\sin(\theta(t)) \\ A\sin(\alpha(t)) \end{bmatrix} \tag{3}$$

where $B(t)$ is the magnetic flux density vector, $B_x(t)$, $B_y(t)$, and $B_z(t)$ are the three-dimensional components along x, y, and z axes, respectively. A is the amplitude, $\theta(t)$ is the heading angle in the X-Y plane to the x-axis, and $\alpha(t)$ is the angle along the z-axis from the X-Y plane. $\theta(t)$ and $\alpha(t)$ are the variables changing

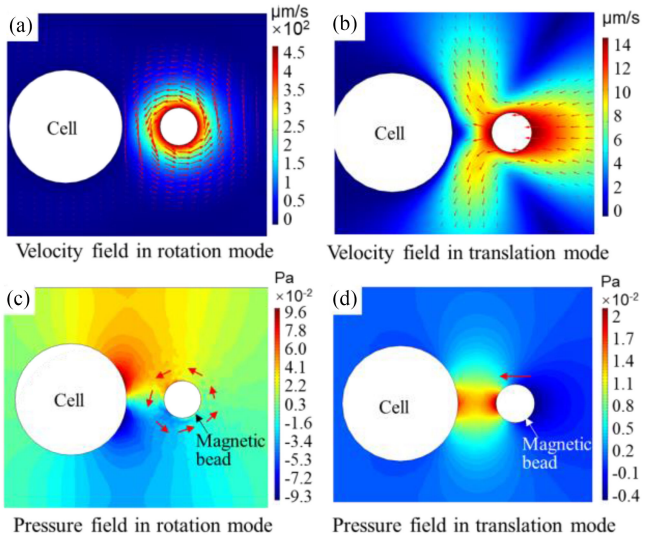

Fig. 3. The simulation of flow field induced by a magnetic bead moving with 5 μm distance between target cell in rotation mode (a) under rotating magnetic filed of 30 Hz and in translation mode (b) with a magnetic bead speed of 14 μm/s. (c) and (d) the simulative pressure induced by the flowing fluid in (a) and (b). Red arrows show the direction of flowing fluid velocity.

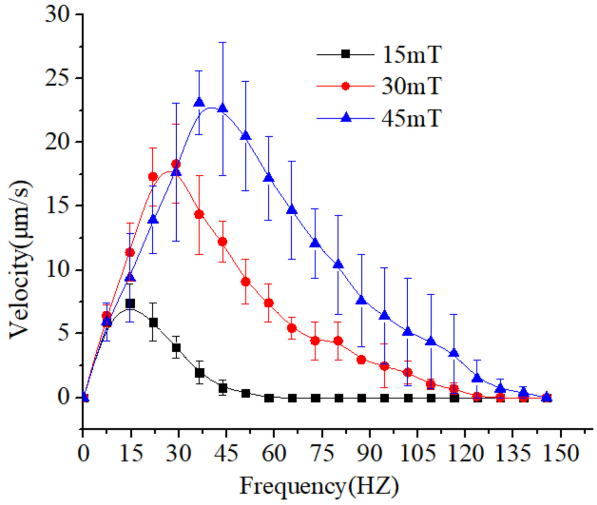

Fig. 4. Relationship between the magnetic bead velocity and the frequency under various magnetic flux density in rotation motion mode. There are 5 sets of data for each situation.

with time at a specific frequency. According to $B(t)$ changes, unique motion modes, and orientation of magnetic beads can be achieved.

To better understand the process and the mechanism of the two motion modes when the magnetic bead approaches the surface of a target cell, we further performed the simulation of the fluid flow fields around the magnetic bead by using a rotating machinery module and fluid-structure-interaction module of COMSOL Multiphysics. The magnetic bead and cell are modeled as the spheres with a diameter of 4.7 μm and 15 μm. Fig. 3(a) and (c) showed the distribution of the fluid field (Y-Z plane) by the rolling magnetic bead (30 Hz). As shown in Fig. 3(c), when the rolling magnetic bead is approaching the cell, a pushing force is produced by the difference in pressure acting on either side of the cell. In this case, the rolling magnetic bead cannot continue to move toward the cell. In contrast with the rotation mode, the simulation results in Fig. 3(b) and (d) reveal the flow velocity and pressure distributions of the magnetic bead in translation mode with a speed of 14 μm/s. As shown in Fig. 3(d), when the translational bead approaches the cell, a pushing force is also produced by the pressure around the cell. However, the pressure is relatively low compared with the simulation result in rotation mode, and the magnetic force acting on the magnetic bead is big enough to overcome this pressure, creating opportunities for a controlled magnetic bead moving to the surface of the cell. Besides, according to the simulations, when the bead cannot continue moving forward in rotation mode, the gap between the bead and the target cell is about 5 μm.

B. Analysis of Key Parameters

To achieve high-speed movement and high-efficiency measurement, the velocity of the magnetic beads moving in rotation mode should be investigated. The statistical results of the relationship between the velocity and the frequency of the magnetic beads under various magnetic flux densities in rotation motion mode were shown in Fig. 4. It was demonstrated that under the same rotating magnetic flux density, the velocity of the magnetic beads rolling along the surface first went up proportionately with frequency growing and reached a maximum value. However, with a further increase of the rotation frequency and beyond a certain threshold, the rolling velocity along the surface of the substrate exhibited a downtrend. According to comprehensive analysis, the main reason for the variation tendency of moving velocity is that at relatively low rotational frequencies, the increased rotation rate of magnetic beads corresponds to an increased interacting number between beads and surface, resulting in the increased moving velocity. After the rotating magnetic field goes through the frequency threshold, the duration of interaction between a magnetic bead and the surface will decrease, which reduces the possibility of torque-generating events. Frequent slippage of magnetic beads will also occur concomitantly, resulting in slower rolling speed at high rotation frequencies. Interestingly, a series of peak velocities under the threshold frequency increased with the magnetic flux density increasing. As a result, the maximum rolling velocity could be 23 μm s^{-1} with a frequency of 45 Hz and a magnetic flux density of 45 mT.

IV. Modeling

A. Force Calibration

As the analysis above, the translation mode should be employed to drive beads toward and squeeze the cell. Therefore, it is necessary to study the magnetic force on the beads quantitatively in the translational state and then calculate the extrusion force on cells.

It is theoretically possible to calculate the force exerted on a magnetic bead in a known field profile. However, inherent inaccuracies in the physical and geometrical properties of the system components make this approach rather impractical. For magnetic beads in microscale, the Reynolds number is typically

minuscule ($Re < 10^{-5}$). Therefore, the flow is laminar and viscous resistance of fluid is dominant, compared with other effects of hydrodynamics. Due to the small mass of the magnetic beads, the velocity could increase quickly with a large acceleration, and the fluid resistance will also increase concomitantly. Soon the magnetic force and the fluid resistance could keep balanced, and the speed begins to remain stable. Consequently, to calibrate the magnetic force, we can calculate the balancing fluidic drag force by tracking the movement of a magnetic bead in stationary fluids of calibrated viscosity. Combined with Stokes' law, the magnetic force F_m and fluidic drag force F_f can be expressed by [34]

$$F_m = F_f = 6\pi\eta r v \tag{4}$$

where η is the fluid viscosity, r is the radius of the magnetic bead, and v is the speed of the magnetic bead.

According to the law of magnetism, the magnetic gradient is greatly affected by the distance between the electromagnet iron core and the magnetic bead. In this letter, to ensure calibration accuracy, the generate magnetic force was calibrated by tracking the displacement and measuring the velocity of magnetic beads in cell suspension solution (20.2 °, 1 mPa·s) in real time when magnetic beads are moving close to the cell surface in the translation mode.

Besides, as the bead began to push the cell and came to a static measurement state, the center of the bead and the cell were in the same plane, so the bead is not in contact with the upper and lower surfaces, and the magnetic force on the bead was balance with the cell support force. The gravity and buoyancy of the bead in the vertical direction were similar and obviously less than the magnetic force, which did not affect the measurement of the mechanical properties of the cells. Therefore, we thought all the magnetic force applied to the magnetic bead was transferred to the cells via pushing.

B. Mechanical Measurement

The measurement mechanism was as same as mechanically characterizing the single cell by the AFM with spherical probe and microbeads driven by optical tweezer [35], [36]. Our magnetically operated microbeads were maintained in a phosphate solution. Measurement of cell mechanical properties only used the pressing process, which was enough for evaluating Young's modulus. The influence of the adhesive force between the cell and the magnetic beads on the measuring results was weak in the pressing process and not considered in the experiments. Thus, when the extrusion force is applied to deform the target cells or other intracellular structures by a magnetic microbead, the experimental force-deformation curve is fitted with the Hertz contact mechanics model that is expressed as follows, after simplification.

$$F = \frac{4}{3} \cdot \frac{E R^{\frac{1}{2}} \delta^{\frac{3}{2}}}{1 - \upsilon^2} \tag{5}$$

where cells are treated as a homogenous, smooth medium. F is the applied load force. E is Young's modulus of the target cells used to measure the mechanical property, v is the Poisson ratio, R is the radius of the magnetic bead, and δ is the deformation caused by the load force. To produce an observable deformation under optical microscopy, δ should be larger than 0.1 μm in the experiments.

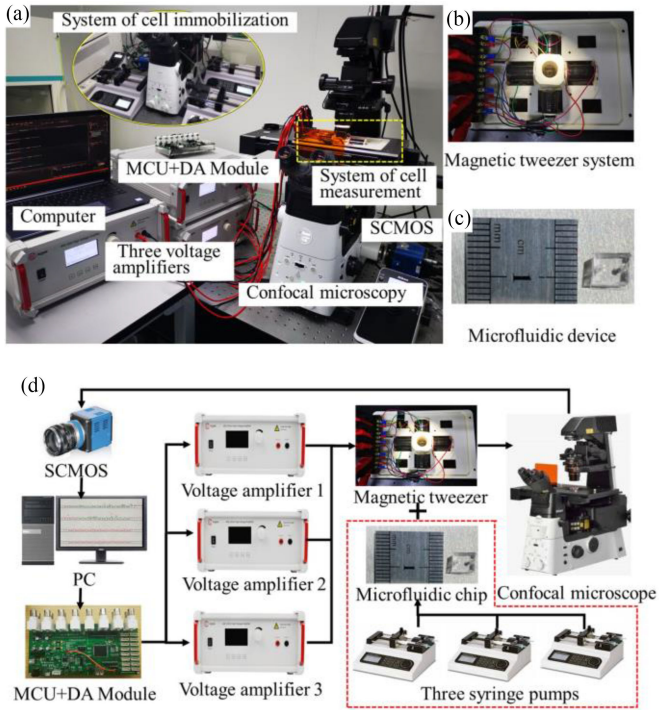

Fig. 5. System Setup. (a) The experimental system for cell mechanical measurement. The insert image shows the experimental system for cell immobilization in microfluidic device. (b) The operated platform of magnetic tweezer including four coils in X-Y plane and a vertical coil along Z direction. (c) Microfluidic device placed in the center of magnetic tweezer platform. (d) Experimental configuration of magnetic tweezer system.

V. Experiments and Results

A. System Setup and Magnetic Tweezer Detail

The experimental system setup for the cell mechanical measurement is shown in Fig. 5. Before magnetic controlling manipulation, three syringe pumps (LSP02-1B) were used for the preparation works in the microfluidic device as introduced in Section II (Fig. 5(d) and insert image in Fig. 5(a)). The experiments were operated under the confocal microscope (Nikon ECLIPSE TI2-E) with a 20× objective (NA: 0.75) for sample imaging. The magnetic beads were prepared by coating chromium dioxide onto uniform polystyrene particles. They were ferromagnetic particles (4.7 μm) and purchased from the company of Spherotech. In the operating platform of the magnetic tweezer (Fig. 5(b)), four coils in X-Y plane were embedded, allowing a total working distance of 5×5 mm^2 for the microfluidic device at the center of the system (Fig. 5(c)). Besides, there were 15000 turns per coil in X-Y plane and 20000 turns per coil in the Z direction to make up for the weakening of magnetic flux density induced by lacking soft-magnetic material inside. In the controlling process, the controlling signal applied to the coils was first generated by a customized program in PC and transported through a serial port to the DA converter (AD5363) that was manually integrated on the control panel (STM32F767ZI). Finally, the power amplifiers (Aigtek ATA-2022H China) were

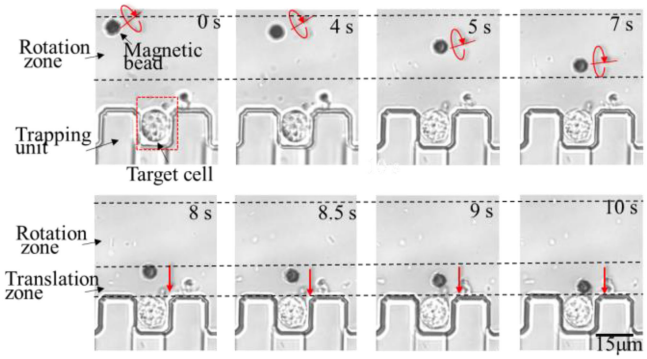

Fig. 6. Demonstration of the magnetic bead movement approaching the target cell in two motion modes in the microfluidic device.

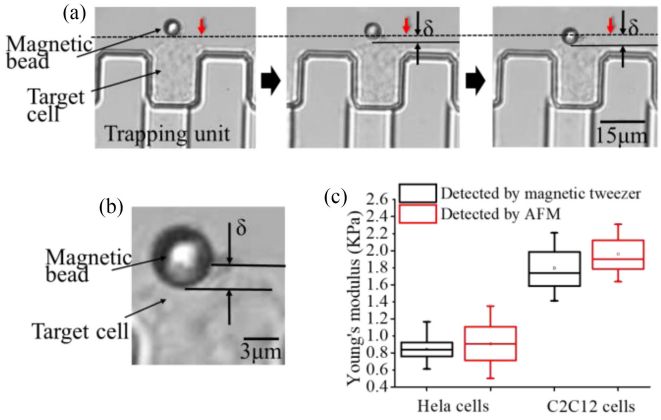

Fig. 7. Experimental results of cell mechanical measurement. (a) Experimental process of the magnetic bead squeezing a measured cell. (b) Partial enlarged drawing of cell deformation. (c) Young's modulus of Hela cells and C2C12 cells detected by magnetic tweezers and AFM, respectively. n = 20 cells.

used to amplify the signal and generated outputs for each coil to create given magnetic fields. All the experimental process was recorded using a CMOS camera (pco.edge 4.2 LT) that offered the framerate up to 100 fps under a maximum resolution of 2048 × 2048 to show the image processing.

B Experimental Results

Based on the previous introduction of the method of mechanical measurement for the single cell in Section II, in the experiments, the Hela cells were immobilized in the trapping units of the microfluidic device, and magnetic beads were introduced into the main channel. As shown in Fig. 6, the process of magnetic beads approaching cells was divided into two steps: approaching cell in rotation mode at a distance and approaching cell in translation mode at close range. It took about 10 s that the beads moved under the magnetic force from their initial position to a target location. As the beads approached the cell in rotation mode at a distance, and the gap between the bead and the cell surface was about 5 μm according to statistics, the magnetic bead rotated with no actual forward movement and can only move in the absolute slipping. The statistic results were the same as the critical value in simulation results, proving the veracity of experiments. It then took about 2 s for the cell to touch the target cell surface at close range. This was of great significance for planning the bead motion path and reducing the movement time of beads in the whole process.

Time-lapse optical microscopy images in Fig. 7(a) demonstrated the typical experimental process of the mechanical measurement by squeezing the target cell with a magnetic bead. In the electromagnet gradient field, the load force was applied to cells by the magnetic bead in translation mode. The measurement of a single cell was repeated three times to reduce the measuring errors. The next measurement can be repeated after 1 min until the deformation on the cell membrane is fully recovered by the last squeezing. Finally, the quantitative evaluation of cell indentation was obtained by confocal fluorescence microscopy (Fig. 7(b)). As shown in Fig. 7(c), the apparent Young's modulus of Hela cells calculated by 1 was 0.8 ± 0.2 kPa. With the same experimental setup, the stiffness of the mouse myoblast C2C12 cells has also been tested, and it's Young's modulus was 1.8 ± 0.4 kPa. We found that Young's modulus of C2C12 cells was bigger than two times of Young's modulus of Hela cell, which well matched the conclusion that Hela cancer cell is softer than the common C2C12 cells [37]. Besides, employing AFM (Park System, NX12,) with the probe modified by the magnetic microbead used in our experiments, we have also tested the stiffnesses of mouse myoblast C2C12 cells and Hela cells [38]. As the results shown in Fig. 7(c), Young's modulus of HeLa cells was 0.75 ± 0.4 kPa, and Young's modulus of C2C12 cells was 2 ± 0.3 kPa. There was a big overlap between Young's modulus data obtained through the proposed magnetic tweezers and the commercialized AFM. Considering the variabilities of the magnitude of the applied stress, stress loading velocity, AFM probe length, and substrates used for cell growth could all influence the detection precision, we thought that Young's modulus of the cells measured by the proposed method in this letter is dependable.

VI. Conclusion

We have demonstrated a system that integrated magnetic tweezers on a cell arraying microfluidic device for efficient single-cell mechanical measurement. Two motion modes of magnetically actuated magnetic beads were introduced and analyzed. The magnetic bead could approach the measuring cell at a distance in rotation mode, while the bead could approach the surface of the target cell at close range in the translation mode. Different distributions of the flow fluid fields around cells induced by moving the magnetic bead in two motion modes were analyzed in the computer simulations. The key parameter analysis of rotation mode was also studied to achieve high-speed motion and efficient measurement. In the two motion stages, the magnetic bead successfully and efficiently moved to a target location and applied load force on the cells. Finally, Young's modulus of Hela cells and C2C12 cells were calculated in preliminary experiments. Compared to the measurement results with AFM, we thought that Young's modulus of the cells measured by the proposed method is dependable.

In the future, we will apply the proposed system in the mechanical characterization of more cell samples, especially the suspended cells. Moreover, we try to utilize the magnetically controlled microbeads to conduct more operations, including translocating the trapped cells using adhesion force and generating a vortex for noncontact manipulation based on fast rotation. We envision the proposed on-chip platform with integrated magnetic tweezer could be an efficient all-purpose tool in biological research at the single-cell level.

REFERENCES

[1] R. A. Harouaka, M. Nisic, and S.-Y. Zheng, "Circulating tumor cell enrichment based on physical properties," *Bone*, vol. 23, no. 1, pp. 1–7, 2008.

[2] V. Swaminathan, K. Mythreye, E. O'Brien, A. Berchuck, G. Blobe, and R. Superfine, "Mechanical stiffness grades metastatic potential in patient tumor cells and in cancer cell lines," *Cancer Res.*, vol. 71, pp. 5075–5080, 2011.

[3] S. Suresh, "Biomechanics and biophysics of cancer cells," *Acta Biomaterialia*, vol. 3, no. 4, pp. 413–438, 2007.

[4] M. Alshareef *et al.*, "Separation of tumor cells with dielectrophoresis-based microfluidic chip," *Biomicrofluidics*, vol. 7, pp. 11803–11816, 2013.

[5] E. Corbin, F. Kong, C. T. Lim, and W. King, "Biophysical properties of human breast cancer cells measured using silicon MEMS resonators and atomic force microscopy," *Lab a chip*, vol. 15, pp. 839–847, 2014.

[6] K. Tomankova, P. Kolar, and J. Malohlava, "Mechanical characterisation of hela cells using atomic force microscopy," in *Current Microscopy Contributions Advances Science Technology*, pp. 549–554, 2012.

[7] X. Guo, K. Bonin, K. Scarpinato, and M. Guthold, "The effect of neighboring cells on the stiffness of cancerous and non-cancerous human mammary epithelial cells," *New J. Phys.*, vol. 16, 2014, Art. no. 105002.

[8] Y. Zheng, J. Wen, J. Nguyen, M. Cachia, C. Wang, and Y. Sun, "Decreased deformability of lymphocytes in chronic lymphocytic leukemia," *Sci. Rep.*, vol. 5, 2015, Art. no. 7613.

[9] N. Gavara, "A beginner's guide to atomic force microscopy probing for cell mechanics," *Microsc. Res. Technique*, vol. 80, pp. 75–84, 2016.

[10] F. Jiang, D. Lin, F. Horkay, and N. Langrana, "Probing mechanical adaptation of neurite outgrowth on a hydrogel material using atomic force microscopy," *Ann. Biomed. Eng.*, vol. 39, pp. 706–713, 2010.

[11] X. Yun *et al.*, "Interrogation of drug effects on hela cells by exploiting new AFM mechanical biomarkers," *RSC Adv*, vol. 7, pp. 43764–43771, 2017.

[12] E. Wojcikiewicz, X. Zhang, and V. Moy, "Force and compliance measurements on living cells using atomic force microscopy (AFM)," *Biol. Procedures Online*, vol. 6, pp. 1–9, 2004.

[13] W. Liang *et al.*, "Recent advances in AFM-based biological characterizations and applications at multiple levels," *Soft Matter*, vol. 16, no. 39, pp. 8962–8984, 2020.

[14] S. Vichare, S. Sen, and M. M. Inamdar, "Cellular mechanoadaptation to substrate mechanical properties: Contributions of substrate stiffness and thickness to cell stiffness measurements using AFM," *Soft Matter*, vol. 10, no. 8, pp. 1174–1181, 2014.

[15] M. Brandão *et al.*, "Optical tweezers for measuring red blood cell elasticity: Application to the study of drug response in sickle cell disease," *Eur. J. Haematol.*, vol. 70, pp. 207–211, 2003.

[16] Y. Tan, D. Sun, J. Wang, and W. Huang, "Mechanical characterization of human red blood cells under different osmotic conditions by robotic manipulation with optical tweezers," *IEEE Trans. Bio-Med. Eng.*, vol. 57, no. 7, pp. 1816–1825, Feb. 2010.

[17] H. Zhang and I. K.-K. Liu, "Optical tweezers for single cells," *J. Roy. Soc., Interface / Roy. Soc.*, vol. 5, pp. 671–690, 2008.

[18] S. Khakshour, T. V. Beischlag, C. Sparrey, and E. J. Park, "Mechanical characterization of ART-treated jurkat cells using optical tweezers," in *Proc. 36th Annu. Int. Conf. IEEE Eng. Med. Biol. Soc.*, 2014, pp. 6806–6809.

[19] C. H. D. Tsai, M. Kaneko, and F. Arai, "Evaluation of cell impedance using a μ-channel," in *Proc. Annu. Int. Conf. IEEE Eng. Med. Biol. Soc.*, 2012, pp. 5518–5521.

[20] C. H. D. Tsai, M. Kaneko, S. Sakuma, and F. Arai, "Phase decomposition of a cell passing through a μ-channel: A method for improving the evaluation of cell stiffness," in *Proc. IEEE Int. Conf. Mechatronics Automat., 2012*.

[21] C.-H. Tsai, M. Kaneko, S. Sakuma, and F. Arai, "Observability of cell stiffness in micro-channel method," in *Proc. - IEEE Int. Conf. Robot. Automat.*, 2013, pp. 2807–2813.

[22] C. H. D. Tsai, S. Sakuma, F. Arai, and M. Kaneko, "A new dimensionless index for evaluating cell stiffness-based deformability in microchannel," *IEEE Trans. Biomed. Eng.*, vol. 61, no. 4, pp. 1187–1195, Apr. 2014.

[23] A. Adamo, A. Sharei, L. Adamo, B. Lee, S. Mao, and K. Jensen, "Microfluidics-Based assessment of cell deformability," *Anal. Chem.*, vol. 84, pp. 6438–6443, 2012.

[24] D. Gossett *et al.*, "Hydrodynamic stretching of single cells for large population mechanical phenotyping [Internet]," *Proc. Nat. Acad. Sci. United States America*, vol. 109, pp. 7630–7635, 2012.

[25] S. Youn, D. W. Lee, and Y. Cho, "Cell-Deformability-Monitoring chips based on strain-dependent cell-lysis rates," *J. Microelectromech. Syst.*, vol. 17, no. 2, pp. 302–308, 2008.

[26] H. W. Hou, Q. S. Li, G. Y. H. Lee, A. P. Kumar, C. N. Ong, and C. T. Lim, "Deformability study of breast cancer cells using microfluidics," *Biomed. Microdevices*, vol. 11, no. 3, pp. 557–564, 2009.

[27] S. Byun *et al.*, "Characterizing deformability and surface friction of cancer cells," *Proc. Nat. Acad. Sci. United States America*, vol. 110, no. 19, pp. 7580–7585, 2013.

[28] X. Fan *et al.*, "Automated noncontact micromanipulation using magnetic swimming microrobots," *IEEE Trans. Nanotechnol.*, vol. 17, no. 4, pp. 666–669, Jul. 2018.

[29] M. Irmscher, A. M. De Jong, H. Kress, and M. W. J. Prins, "Probing the cell membrane by magnetic particle actuation and euler angle tracking," *Biophysical J.*, vol. 102, no. 3, pp. 698–708, 2012.

[30] O. Yasa, P. Erkoc, Y. Alapan, and M. Sitti, "Microalga-Powered microswimmers toward active cargo delivery," *Adv. Mater.*, vol. 30, no. 45, pp. 1–10, 2018.

[31] K. Chung, C. Rivet, M. Kemp, and H. Lu, "Imaging single-cell signaling dynamics with a deterministic high-density single-cell trap array," *Anal. Chem.*, vol. 83, pp. 7044–7052, 2011.

[32] Q. Huang, S. Mao, M. Khan, and J. Lin, "Single-cell assay on microfluidic devices," *Analyst*, vol. 144, pp. 808–823, 2019.

[33] X. Tang *et al.*, "On-Chip cell–cell interaction monitoring at single-cell level by efficient immobilization of multiple cells in adjustable quantities," *Anal. Chem.*, vol. 92, no. 17, pp. 11607–11616, 2020.

[34] M. Tanase, N. Biais, and M. Sheetz, "Magnetic tweezers in cell biology," *Methods Cell Biol*, vol. 83, no. 07, pp. 473–493, 2007.

[35] J. Zemła, J. Danilkiewicz, B. Orzechowska, J. Pabijan, S. Seweryn, and M. Lekka, "Atomic force microscopy as a tool for assessing the cellular elasticity and adhesiveness to identify cancer cells and tissues," *Semin. Cell Dev. Biol.*, vol. 73, pp. 115–124, 2018.

[36] Y. Tan, D. Sun, J. Wang, and W. Huang, "Mechanical characterization of human red blood cells under different osmotic conditions by robotic manipulation with optical tweezers," *IEEE Trans. Biomed. Eng.*, vol. 57, no. 7, pp. 1816–1825, Jul. 2010.

[37] L. Huang, F. Liang, Y. Feng, P. Zhao, and W. Wang, "On-chip integrated optical stretching and electrorotation enabling single-cell biophysical analysis," *Microsystems Nanoeng*, vol. 6, no. 1, pp. 57–71, 2020.

[38] E. Moeendarbary *et al.*, "The cytoplasm of living cells behaves as a poroelastic material," *Nat. Mater.*, vol. 12, no. 3, pp. 253–261, 2013.